SELF-PROPELLED EEL-LIKE BODY DYNAMICS : SIMPLIFIED MODEL AND OPTIMISATION OF LAWS OF DEFORMATION

Leroyer Alban & Michel Visonneau
Ecole Centrale Nantes, Nantes, France

Mathieu Porez & Frédéric Boyer
Ecole des Mines de Nantes, Nantes, France

ABSTRACT

This paper is devoted to a simplified model for the simulation of self-propelled eel-like body. After a description of this model based on an extension of the Lighthill theory, it is explained how Navier-Stokes simulations have been used to calibrate and to validate it. In a second part, the parameterization of laws of deformation is under consideration to be optimized, using efficiency as cost function.

1. INTRODUCTION

Among numerous species which can be observed in Nature, fishes have always fascinated human beings with their incredible ease to couple instinctively Newton's laws and Navier-Stokes equations in order to swim. The efficiency and the great maneuvrability of their locomotion function developed during their evolution compose a tremendous application field for fluid engineering illustrated by the growing number of related biomimetic studies. During few last years, a French project (ROBEA followed by an ANR project RAAMO) has been started to design an efficient autonomous flexible underwater eel-like robot (see Figure 1). In this framework, some developments have been done and previously presented in FIV2004 to achieve Navier-Stokes simulations of such a self-propelled fish-like body (see Leroyer & Visonneau, 2004, 2005). In the same time, a simplified model has been designed to have a real time simulator capable to be used for the control. The proposed model is based on Lighthill's original "Large Amplitude Elongated Body Theory", denoted L.A.E.B.T. (see Lighthill, 1960, 1969), but both extended to 3-D and to take into account viscous effects.

In a first part, the hypothesis of the model are detailed, so as the calibration and validation procedures using the reference database coming from the Navier-Stokes solver. Then, the second part is devoted to first attempts concerning optimisation of deformation laws.

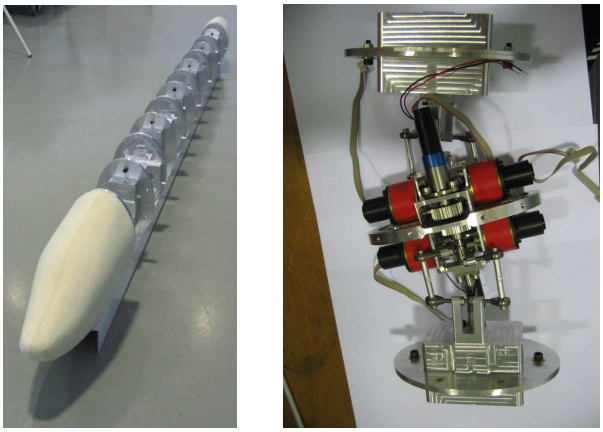

(a) Global view (b) Detail of a vertebrae

Figure 1: views of the prototype

2. SIMPLIFIED MODEL AND NAVIER-STOKES SIMULATIONS

2.1. Description of the simplified model

Let's consider an elongated fish-like body of length L, whose back-bone is represented by a curvilinear coordinate $X_1 \in [0, L]$. The L.A.E.B.T. of Lighthill is based under the following assumptions:

• The fluid is first of all considered as inviscid, incompressible and is irrotational everywhere except on a free vortex sheet shedded from the sharp trailing edge of the caudal fin. Still following Lighthill, the wake is then isolated from the flow laterally surrounding the fish by a geometric plane π orthogonal to the fish backbone and passing through the trailing edge. Hence, only the fluid contained in the control volume $\mathcal{D}$ of figure 2 is considered.

• Due to the slender geometry of the fish (and the robot), the fluid flow in $\mathcal{D}$ is approximated

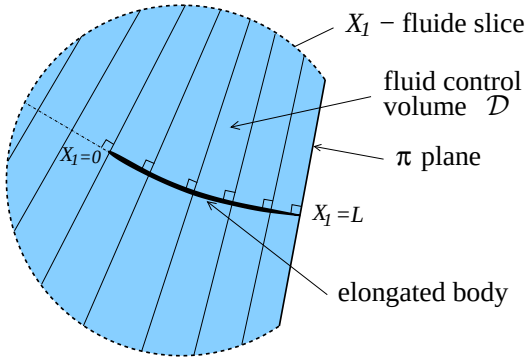

Figure 2: definition of the fluid control volume

by a stratification of planar potential flows transverse to the fish back-bone (cf. figure 2). Hence, each of these flow slices induces a lineic transversal effort acting on the body which can be expressed by added mass terms.

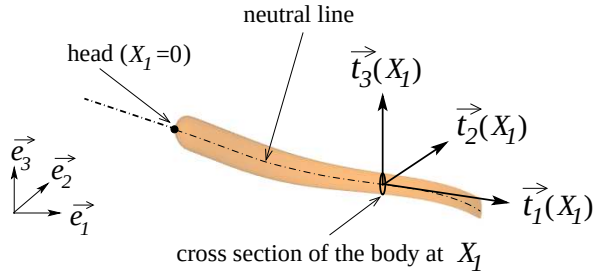

Figure 3: definition of the body axis

Under these hypotheses, the momentum conservation law, written on the half space fluid domain $\mathcal{D}$ following the body during its motion, finally leads to a distribution of reactive lineic fluid forces and torques acting all along the body and a propulsive term represented here by a punctual force acting at the tail. Formulae for 3-D deformation are not described here since the optimization only concerns planar deformation (see Boyer et al. (2007b,a) for a complete description of the model). In the case of planar deformation (and motion), the curvature vector is aligned with $\overrightarrow{t_3}$, $\overrightarrow{t_3}$ remains identical equal to the fixed vector $\overrightarrow{e_3}$ of the reference frame, and $(\overrightarrow{t_1}, \overrightarrow{t_2})$ remain a linear combination of $(\overrightarrow{e_1}, \overrightarrow{e_2})$ (see figure 3). The distribution of fluid forces is then only reduced to a lineic force $\overrightarrow{f_{rt}}$ along the body and a propulsive term denoted by $\overrightarrow{F_{rT}}$ with the following expressions (see also figure 4):

- $\overrightarrow{f_{rt}} = -m_{a2} \dfrac{d(v_2\, \overrightarrow{t_2})}{dt}$,
- $\overrightarrow{F_{rT}} = \left[v_1\, m_{a2}\, v_2\, \overrightarrow{t_2} - \frac{1}{2}\, m_{a2}\, v_2^2\, \overrightarrow{t_1} \right]_{X_1=L}$,

with m_{a2} the added mass of the 2-D section through $\overrightarrow{t_2}$ and $\overrightarrow{v} = v_i\, \overrightarrow{t_i}$ the velocity of the centre of the considered body section.

In order to improve the accuracy of the dynamics, a supplementary added mass concentrated force applied onto the nose $\overrightarrow{F_{rH}}$ has been added to model the action of the axial relative flow with respect to the body (this reactive force can not exist in the Lighthill theory since the flow is supposed not to be disturbed axially) : $\overrightarrow{F_{rH}} = -M_{a1} \dfrac{dv_1}{dt}(0)\, \overrightarrow{t_1(0)}$.

Finally, the resultant of the whole distribution of fluid force $\overrightarrow{F_{f\to b}}$ on the body can then be expressed by equation 1. Resultant torque at the point O_1 where the Newton's laws are solved can also be evaluated using the balance of angular momentum on the same control volume $\mathcal{D}$ (see equation 2). More details on the whole model can be found in Boyer et al. (2007b,a).

$$\overrightarrow{F_{f\to b}} = \int_0^L \overrightarrow{f_{rt}}(X_1) dX_1 + \overrightarrow{F_{rT}} + \overrightarrow{F_{rH}} \qquad (1)$$

$$\overrightarrow{M_{f\to b}}(O_1) = \frac{d}{dt} \int_0^L \overrightarrow{O_1P} \otimes m_{a2}\, v_2\, \overrightarrow{t_2} dX_1 + \overrightarrow{O_1H} \otimes \overrightarrow{F_{rH}} + \overrightarrow{O_1H} \otimes \overrightarrow{F_{rT}} \qquad (2)$$

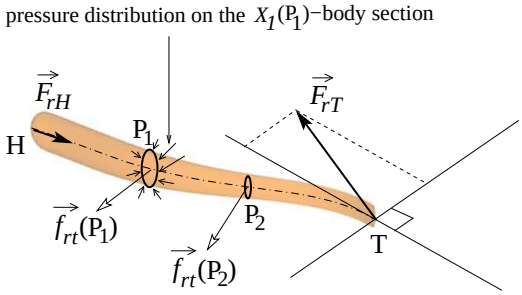

Figure 4: modelled reactive forces

In order to integrate more physics in the model and then improve the behaviour of the previous "pure reactive model" with respect to the reality, two corrections have been added to it. The first one complies with the slender body theory by modeling the pressure and viscous drag forces slice by slice. It is done through two lineic forces $\overrightarrow{f_{vt}}$ and $\overrightarrow{f_{vl}}$, respectively transversal and longitudinal to the cross section (see figure 5). Their expression are given as follows :

$$\overrightarrow{f_{vt}} = -\frac{1}{2} \rho\, \mathcal{H}\, C_{d2}\, |V_2|\, V_2\, \overrightarrow{t_2}$$

$$\overrightarrow{f_{vl}} = -\frac{1}{2} \rho\, \mathcal{P}\, C_f\, |V_1|\, V_1\, \overrightarrow{t_1}$$

where $\mathcal{H}$ and $\mathcal{P}$ are respectively the height and the perimeter of the X_1 cross section (which in our case is elliptic). ρ represents the density of the fluid. C_f is the non-dimensional axial friction coefficient, and C_{d2} is the non-dimensional drag coefficient for a motion along $\overrightarrow{t_2}$ of the considered section.

The second correction consists in modeling the local resistance due to the rounded nose by a punctual force $\overrightarrow{F_{vH}}$ applied at $X_1 = 0$ (see figure 5). Its general expression is deduced from experimental fluid mechanics (Hoerner, 1965):

$$\overrightarrow{F_{vH}} = -\frac{1}{2}\rho\, C_p\, \mathcal{S}\, |V_1(0)|\, V_1(0)\, \overrightarrow{t_1}(0)$$

with $\mathcal{S}$ the aera offered to the fluid when the eel moves axially, i.e. the area of the projection of the surface of the head onto the plane normal to $\overrightarrow{t_1}(0)$.

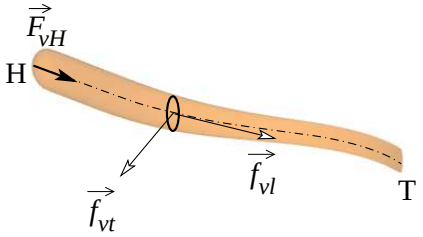

Figure 5: modelled viscous effects

2.2. Calibration of the model

For the moment, the model has been calibrated using a temporary shape of a one meter length body with elliptic cross-sections varying along the body. Details on the analytical description of the shape can be found in Boyer et al. (2007a).

In accordance with the previous developments, four parameters have to be specified, i.e.: the axial viscous drag coefficient C_f, the pressure drag C_p related to the rounded nose of the head, the transverse pressure drag C_{d2} and the axial added mass coefficient M_{a1}. In order to fix all these parameters, the following "identification process" has been pursued, by using both analytical and experimental data of fluid mechanics and CFD results on basic cases :

Identification of C_f : this coefficient is simply based on classical boundary-layer relation for a flat plate (Blasius and Von Karman formulae, respectively, for laminar and turbulent regimes). These relations only depend on the local longitudinal Reynolds number, denoted by $\mathcal{R}e_{X_1//}$. Keeping in mind the fact that the transition phenomena is not yet taken into account correctly in the Navier-Stokes solver, RANSE simulations of flow around around a 2-D thin flat plate were performed to fix the numerical Reynolds number transition (see figure 6). The law of C_f is finally described by :

$$\mathcal{R}e_{X_1//} \leq 8.10^4 \ , \ C_f = 0.664/\mathcal{R}e_{X_1//}^{0.5}$$

$$\mathcal{R}e_{X_1//} > 8.10^4 \ , \ C_f = 0.059/\mathcal{R}e_{X_1//}^{1/5}$$

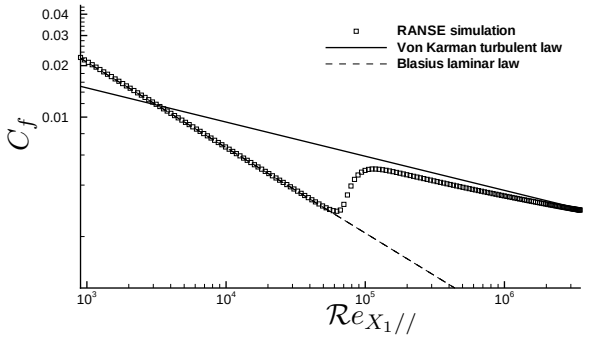

Figure 6: C_f coefficient on a 2-D thin flat plane

Identification of C_p : this coefficient was identified by comparing the Navier-Stokes simulation to those provided by the simplified model for a gait in which the fish is released with an initial forward speed ($1L/s$) in a straight and rigid configuration. The friction drag being known by the evolution of C_f previously defined, this case enables to simply calibrate C_p to have a similar reduction of the forward velocity. $C_p = 0.036$ leads to quasi-superimposed curves in our case.

Identification of C_{d2} : like a flow around oscillating cylinder, C_{d2} should be time-dependent on the transverse Reynolds and the Keulegan-Carpenter numbers (see Sarpkaya, 1986). But the problem is here quite different from studies which can be found in the literature : due to the the forward fish motion, the flow perturbations generated by a given cross-section no longer influence the section itself but rather the neighboring sections along the beam axis. Furthermore, the amplitude of oscillations changes when moving along the body, and sections do not have circular profiles but elliptic ones for which fewer experimental data are available. Hence, guided by simplicity but keeping the right order of magnitude of this transverse force, a constant value of 1.98 was chosen for C_{d2} (in accordance with the experimental data of Hoerner (1965) for a 2-D transverse flat plate plunged in a stationary flow, corresponding to the orders of magnitude of the transverse Reynolds obtained with the tested body).

Identification of M_{a1} : with the adopted geometry of the head, an half axial added mass of an ellipsoid enduring a translation along its principal axis was taken for M_{a1}, i.e. $\rho\, k\, \frac{2\pi}{3} abc$, where $k = 0.32$ is a dimensionless value analytically computed by Lamb (1932), and $2a, 2b$ and $2c$ are the axis lengths of the ellipsoid.

2.3. Validation of the model

This fluid force model has been programmed in C++ coupling to a Cosserat beam theory (Boyer & Primault, 2004) to solve the dynamics of the robot and to the reach the internal torques (Boyer et al., 2007a, 2006). In fact, the eel is here considered as a non-linear beam controlled continuously along its material axis. It has also been integrated in the Navier-Stokes solver. The self-propelled dynamics of the robot can thus be solved with similar conditions using either the RANSE equations (denoted by N-S) or the simplified model (marked S-M). In all cases, motion of the head results from the solved interaction between the dynamics of the body and the fluid response to the deformation, since only the law of curvature in time is imposed.

2.3.1. reference database from CFD

Navier-Stokes simulations have been performed using ISIS-CFD, developed by the CFD group of the Fluid Mechanics Laboratory of Centrale Nantes. It is dedicated to simulate incompressible fluid flows involving turbulence, free surface and moving bodies. A finite-volume method is used to solve the incompressible unsteady RANS equations under isothermal conditions on unstructured meshes, enabling to deal with complex geometries.

For this specific application, a grid dependence study (with structured and unstructured meshes from 65 000 cells up to 950 000 cells) has been carried out to be sure that the numerical error is under control. The influence of the turbulence model (in both law of wall and near-wall configurations) has also been studied, keeping the same imposed deformation of the body (see Boyer et al. (2007a) for complete results). Differences obtained between all the reached forward velocities do not exceed 5% whatever the grid and the turbulence model used. Consequently, all the simulations for testing different laws of deformation have been performed using the coarser grid (designed for a law of wall turbulence modelling) with the $k-\omega$-SST turbulence model (Menter, 1994). This configuration ensures reasonable CPU time cost and a good ratio of the accuracy over the CPU time cost (in fact accurate enough while keeping in mind that the main objective is to validate the dynamics of the simplified model). Numerical features of the Navier-Stokes solver and of the flow/motion coupling are not detailed here but can be found in Leroyer & Visonneau (2004, 2005).

2.3.2. forward straight-line gaits

For these tests, curvature through $\overrightarrow{t_3}$ has been imposed to : $K_3 = \mathcal{K}(X_1)\sin\left[2\pi\left(\frac{X_1}{\lambda} - \frac{t}{T}\right)\right]$.

A large number of tests (with different period of oscillation T, wave length λ and amplitude $\mathcal{K}$) have been tested using this periodical law of deformation leading to a mean forward speed of the head (marked $\overline{v}_{1,N-S}(0)$ for the Navier-Stokes result and $\overline{v}_{1,S-M}(0)$ for the simplified model).

$$e_{\overline{v_1}} = \frac{|\overline{v}_{1,N-S}(0) - \overline{v}_{1,S-M}(0)|}{|\overline{v}_{1,N-S}(0)|} \qquad (3)$$

Error ratio $e_{\overline{v_1}}$ defined by equation 3 are finally always below 4%, except one (equal to 9%). But, for this one, forward velocity is very small ($\approx 0.3L/s$), and the Reynolds number is then quite low. Consequently, the inviscid fluid assumption is surely less valid and the model of C_f more dependent on the fish deformation.

2.3.3. turning gaits

Other laws of curvature have been tested, especially turning manoeuvres, keeping or not the propulsion during the turning phase (turn is obtained by imposing smoothly a constant curvature along the entire body). Here again, it can be seen that the model is able to capture the same global dynamics of the head, and similar trajectories (figure 7) with respect to the Navier-Stokes simulations. Differences of mean final orientation do not exceed 8% in all tested gaits.

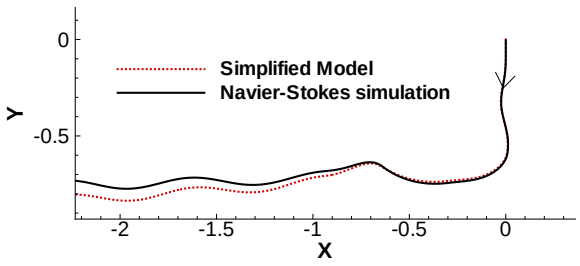

Figure 7: comparison of head trajectory for a turning manoeuvre

3. OPTIMIZATION OF LAW OF DEFORMATION

The simplified model is very economical in terms of CPU time consumption. Thus, it is suited for the on-line command of eel-like robot, but it can also be used for optimization purpose.

3.1. Optimization procedure

The integration of the model in the Navier-Stokes solver enables the use of the optimization tools included in ISIS-CFD. The procedure consists in maximizing a cost function F depending on the flow variables $Q(D)$ and the design variables D. The governing equation of the flow $R(D, Q(D)) = 0$ (here defined by the simplified model) are considered as constraints which must be satisfied at each step of the design cycle. Some bound constraints for D must be added in order to keep realistic solutions. Thus, the variation domain of the design variables is usually closed. From a mathematical point of view, the problem may be expressed as:

$$\text{Maximize } F(D, Q(D)) \text{ constrained to}$$
$$R(D, Q(D)) = 0 \quad \text{with } L_i \leq D \leq L_s$$

Therefore, the design procedure consists in successive gaits with different parameters (or design variables) for the law of deformation whose values are modified by an optimization algorithm. Thus, the design cycle may be described by:

1. Initialization of the design parameters D
2. Simulation of the gait $Q(D)$ until reaching stabilized average values
3. Evaluation of the cost function $F(D, Q(D))$
4. Update of D by the optimization algorithm
5. Goto step (2)

Here, optimizer has been managed by the way of genetic algorithm and simplex method to predict improved design variables at each optimization step. For more details on these algorithms, (see Duvigneau & Visonneau, 2006, 2004).

3.2. Parameters and cost function

Here, only the fluid point of view is considered. The body undulation which is imposed is supposed to be not power consuming and working like a spring-mass system without losses.

Generally, studies about living species extract positions of the body in time with respect to the mean straightline (see Videler (1993) p103). But this information contains both the shape and head motion (only without the forward component, i.e. with the same abscissa for the head). For example, Tytell (1994) gives an analytical lateral deflection with respect to the mean straightline by equation 4.

$$y(X_1, t) = A e^{\alpha\left(\frac{X_1}{L}-1\right)} \sin\left[2\pi\left(\frac{X_1}{\lambda} - \frac{t}{T}\right)\right] \quad (4)$$

For the optimization purpose, the curvature d^2y/dX_1^2 has been imposed to obtain the same deformation as those described by Tytell (1994). But in our case, transversal displacement and orientation of the head in time are not imposed but solved. As our body shape is surely not similar to the real eels studied, it is normal that these solved parameters are finally not superimposed with the analytical position $y(0)$ and orientation $dy/dX_1(0)$ included in the deflection law given by Tytell (1994). However, as it can be seen on figure 8 (corresponding to the initial parameters of the deformation law), the same order of magnitude is found again.

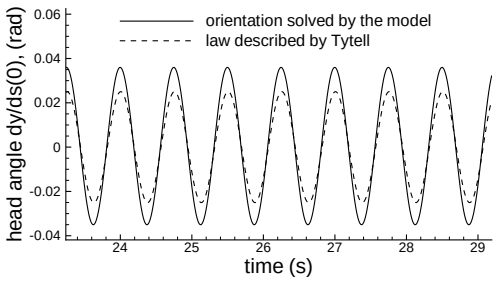

Figure 8: Comparison of head orientation

Design variables D are those appearing in the law of deformation, i.e. : $D = \{A, \alpha, \lambda, T\}$. The cost function is based on an efficiency criteria: optimization aims at maximizing η_f defined by:

$$\eta_f = \frac{F_r\,\overline{v_1}}{\mathcal{P}_f} \quad , \quad \text{with } \mathcal{P}_f = \int_{body} \left[\vec{\vec{\sigma}}\ \vec{n}\right].\vec{v}\,dS$$

where $\overline{v_1}$ means the average forward velocity reached by the self-propelled body and F_r the resistive force for the same rigid shape when towing at the $\overline{v_1}$ velocity. $\mathcal{P}_f$ represents the average power transfered to the fluid to produce the swimming motion ($\vec{\vec{\sigma}}$ means stress tensor, $\vec{n}$ the outer surface normal vector and $\vec{v}$ the velocity of the moving surface).

Some first attempts trying to optimize velocity using parameters like amplitude and frequency have been tested. But they always lead to the highest range of amplitude and frequency, sometimes not realistic if the bounded constraint was chosen very large. On the contrary, with efficiency as the cost function, optimization reaches

D	A (m)	α	λ(m)	T(s)
L_i	0.05	2.5	0.5	0.5
L_s	0.12	3.5	1.5	1.0
initial values	0.08	3.	1.0	0.75
optimized values	0.06	3.4	0.52	0.65

Table 1: *optimization results*

values in the definition domain of parameters. Results of optimization (genetic algorithm followed by simplex method to finalize the optimization) using the simplified model are given on table 1. Initial efficiency is equal to 0.68 whereas optimized value grows up to 0.77. However, trends are not the same concerning velocity ($0.62L.s^{-1}$ for the initial law of deformation against $0.47L.s^{-1}$ for the optimized one). The optimized law give a Strouhal number around of 0.4 which is in the range of those observed among living species (see Tytell, 1994).

4. CONCLUSION

First, this paper aims at describing the simplified model of self-propelled eel-like body. Some comparisons with Navier-Stokes simulations show that the dynamics behaviour is well reproduced, leading us to investigate optimization by using the simplified model which is very low CPU consuming. Design variables, cost function and optimization procedure are then described in the second part. First optimized results are promising, but need now to be controled and validated by a-posteriori CFD computations.

Acknowlegments : the authors gratefully acknowledge the scientific committee of the French National Research Agency which partly supports the RAAMO project.

5. REFERENCES

Boyer, F. & Primault, D., 2004. Finite element of slender beams in finite transformations: a geometrically exact approach. *Int. J. for numerical methods in engineering*, **59**: 669–702.

Boyer, F., Porez, M., & Khalil, W., 2006. Macro-continuous computed torque algorithm for the three-dimensional eel-like robot. *IEEE J. Trans. on Robotics*, **22**: 763–775.

Boyer, F., Porez, M., Leroyer, A., & Visonneau, M., 2007a. Fast dynamics of an eel-like robot, comparisons with Navier-Stokes simulations. *Submitted, Technical Report of Ecole des Mines de Nantes no.07/9/Auto, online available: http://www.irccyn.ec-nantes.fr/hebergement/Publications/2007/3722.pdf.*

Boyer, F., Porez, M., & Leroyer, A., 2007b. Poincaré-Cosserat equations for Lighthill three-dimensional dynamic model of a self propolled eel devoted to robotics. *Submitted, Technical Report of EMN and IRCCyN no.07/8/Auto, online available: http://www.irccyn.ec-nantes.fr/hebergement/Publications/2007/3721.pdf.*

Duvigneau, R. & Visonneau, M., 2004. Hybrid genetic algorithms and artificial neural networks for complex design optimization in cfd. *Int. J. for Numerical Methods in Fluids*, **44/11**: 1257–1278.

Duvigneau, R. & Visonneau, M., 2006. Optimization of a synthetic jet actuator for aerodynamic stall control. *Computers & Fluids*, **35**: 624–638.

Hoerner, S. F., 1965. *Fluid Dynamic Drag.* Hoerner Fluid Dynamics.

Lamb, H., 1932. *Hydrodynamics.* Dover Publication.

Leroyer, A. & Visonneau, M., 2004. Interaction between fluid and self-propelled fish-like motion. *8th International Conference on Flow-Induced Vibrations*, Paris.

Leroyer, A. & Visonneau, M., 2005. Numerical methods for RANSE simulations of a self-propelled fish-like body. *Journal of Fluids and Structures*, **20**: 975–991.

Lighthill, M. J., 1960. Note on the swimming of slender fish. *Journal of Fluid Mechanics*, **9**: 305–317.

Lighthill, M. J., 1969. Hydromechanics of aquatic animal locomotion. *Annual review of Fluid Mechanics*, **1**: 413–446.

Menter, F. R., 1994. Two-equation eddy viscosity turbulence models for engineering applications. *AIAA Journal*, **32**: 1299–1310.

Sarpkaya, T., 1986. Force on a circular cylinder in viscous oscillatory flow at low keulegan-carpenter numbers. *Journal of Fluid Mechanics*, **133**: 265–285.

Tytell, E., 1994. The hydrodynamics of eel swimming ii. effect of swimming speed. *J. Exp. Biology*, **207**: 3265–3279.

Videler, J. J., 1993. *Fish Swimming.* Chapman and Hall. Fish and Fisheries Series 10.